Why EXAFS Underestimated the Size of Small Supported MoS₂ Particles

Takafumi Shido† and Roel Prins*

Laboratory for Technical Chemistry, Swiss Federal Institute for Technology (ETH), 8092 Zurich, Switzerland

Received: May 20, 1998; In Final Form: August 10, 1998

EXAFS spectra of distorted and disordered small MoS₂ particles were simulated by means of the FEFF7 program. The simulated EXAFS spectra of several models were compared with observed EXAFS spectra of small MoS₂ particles which had been characterized by TEM (Calais et al. *J. Catal.* **1998,** *174,* 130). The EXAFS spectra could be reproduced well by a model in which Mo–Mo distances at the edges of the MoS₂ particles are 0.16 Å longer than in bulk MoS₂ and the Mo atom positions are statistically disordered. The simulation demonstrated that the diameter of the MoS₂ slabs and the degree of distortion at the MoS₂ edges cannot be determined simultaneously and that the assumption that Mo atoms in the particles occupy regular positions causes a substantial underestimation of the MoS₂ diameter. A novel function relating the coordination number of the nearest Mo–Mo contribution to the MoS₂ slab diameter is proposed. With this function, the diameter of the MoS₂ slabs, estimated from EXAFS data, agrees with that of TEM data.

I. Introduction

Molybdenum sulfide based catalysts supported on oxidic or carbon carriers are used in the hydroprocessing of petroleum fractions. Several investigations have attempted to elucidate the catalyst properties and structures and to develop a better industrial catalyst.[1–8] The active structure of these catalysts has been investigated extensively by means of extended X-ray fine structure (EXAFS)[3,4,7,9–20] and transmission electron microscopy (TEM).[15,21–33] TEM revealed that Mo is present in the form of small MoS₂ particles consisting of a stack of several MoS₂ slabs. This is basically supported by the EXAFS results which show that the nearest Mo–S and Mo–Mo distances in the particles are typical of MoS₂. The number of slabs cannot be estimated from the EXAFS data, because the stacking between adjacent MoS₂ layers is irregular and the Mo–Mo contribution between the slabs (6.2 Å) overlaps with the multiple scattering contributions of Mo–Mo and Mo–S distances within a slab. On the other hand, the diameter of the slab can be estimated from the coordination number (CN1) of the nearest Mo–Mo contribution (Mo–Mo-1). This determination of the slab diameter, however, revealed a considerable disagreement between EXAFS and TEM. While the average diameter of the MoS₂ slabs, estimated by TEM, was 20–44 Å, that estimated by EXAFS was only about 10 Å. Particle size determination is critical for a proper interpretation of reaction kinetics, because it requires the knowledge of the number of active atoms exposed at the surface. It is, therefore, very important to eliminate the discrepancy between the EXAFS and TEM particle size determinations.

Both EXAFS and TEM have advantages and disadvantages. TEM allows the direct measurement of particle size and particle size distribution. Particles with a diameter less than 20 Å, however, cannot be clearly observed. In addition, the sample is usually dispersed on a grid and, consequently, in situ

measurement is difficult. EXAFS is not a direct method for particle size determination; one has to interpret the obtained coordination numbers. The slab diameter is estimated from the nearest Mo–Mo-1 coordination number (CN1), and a Gaussian distribution of the bond lengths is usually assumed to analyze the data. However, the *CN* is sensitive to the distribution and is lower than its actual value when an asymmetric distribution is present and a normal data analysis is performed.[34–37] This effect can be substantial if the particle size is estimated from the *CN* of a contribution without direct chemical bonding, such as the Mo–Mo contribution of MoS₂, because the atomic distance between nonbonding atoms can show a wide and complex distribution.[38–40] The advantage of EXAFS, on the other hand, is that it is not limited to a certain particle size and that in situ measurements are clearly feasible. EXAFS is the only method which can routinely estimate the particle size in situ, which is critical for the investigation of the dynamic behavior of catalysts during catalytic reactions.

Recently, Calais et al. measured EXAFS spectra of unsupported MoS₂ particles whose size was well characterized by TEM, XRD, and adsorption measurements.[41] They concluded that the diameter of the MoS₂ slabs determined by EXAFS is smaller than the diameter obtained by the other methods. Important features of their EXAFS spectra are that the structural parameters of the nearest Mo–S contribution (Mo–S-1) are close to those of bulk MoS₂ (as observed in many EXAFS studies[3,9–20,41]) and that the peak intensity of the Mo–Mo-1 contribution is smaller than that of the nearest Mo–S contribution (Mo–S-1) in the Fourier-transformed k^3-weighted EXAFS function (FT of $k^3\chi(k)$) for MoS₂ particle diameters up to 107 Å. Furthermore, the CN1 stayed below 5.0 for particle diameters up to 120 Å, and the Mo–Mo-1 EXAFS contribution could be perfectly fitted with one Mo–Mo-1 contribution. In previous EXAFS studies, it was assumed that the CN1 is barely influenced by disorder and that it corresponds directly to the slab diameter. The experimental results[41] demonstrate, however, that the CN1 does not directly correspond to the diameter.

Thus, it is imperative to find out why the results of EXAFS and TEM are contradictory and to establish a better way of

---

* To whom correspondence should be sent. Address: Universitätstrasse 6, CH-8092 Zürich, Switzerland. Telephone: +41 1 632 54 90. Fax: +41 1 632 11 62. E-mail: prins@tech.chem.ethz.ch.
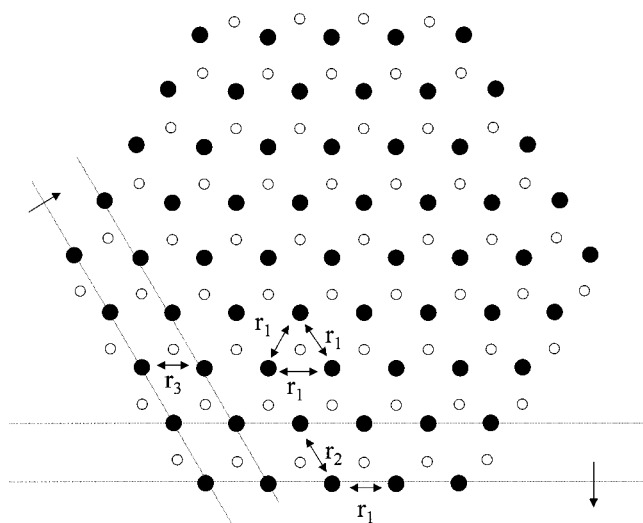† Present address: Department of Chemistry, University of Tokyo, Hongo, Bunkyo-ku, Tokyo 113, Japan.

Why EXAFS Underestimated the Size of MoS$_2$ Particles

J. Phys. Chem. B, Vol. 102, No. 43, 1998 **8427**

Figure 1. Schematic view of the edge distortions of small MoS$_2$ particles. The distances r_1, r_2, and r_3 represent the Mo−Mo distances in the center and the Mo- and the S-terminated edges of the particles, respectively. The r_1 distance was always kept equal to that in bulk MoS$_2$, while r_2 and r_3 were varied.

estimating the diameter of the MoS$_2$ slab so as to gain more insight into hydrotreating catalysis. The goal of this work was to study the effects of the nonideal structure of the MoS$_2$ particles on the EXAFS determination of particle size. In particular, the effects of distortion of the edge of the MoS$_2$ particles by shortening and lengthening of Mo−Mo distances were studied as well as the effects of disorder of the positions of the Mo atoms from the ideal bulk MoS$_2$-like positions. The experimental results in ref 41 will be used to propose a distortion−disorder model which can eliminate the discrepancy between EXAFS and TEM.

II. Method

II.1. Models. In the models that we used to study the influence of edge distortion and Mo disorder, it was assumed that small single MoS$_2$ slabs with a hexagonal symmetry are present on the catalyst surface. Three edges are terminated by S atoms and three by Mo atoms (S- and Mo-terminated edges) as shown in Figure 1. These slabs are, on one hand, distorted at the edges and, on the other, show a statistical disorder of the Mo atoms. The edge distortion is obtained by shifting the edge Mo atoms in the basal plane, perpendicular to the edges. This way, only the Mo−Mo distances between Mo atoms in the outermost and penultimate Mo rows are changed from the MoS$_2$ bulk value (Figure 1). The displacement of the Mo corner atoms is equal to the sum of the displacements of the adjacent edges. Then, the statistical disorder of the Mo atoms was introduced by randomly distributing the Mo atoms in a sphere of a certain radius (r_{max}) around the positions determined by the introduction of the edge distortion. The EXAFS data of MoS$_2$ indicate that the Mo−S-1 distance of the small particles is close to that of bulk MoS$_2$.[3,9−20,41] Therefore, the S atoms were positioned at both sides of the basal plane and in the S-terminated edges, while keeping the Mo−S distance at the bulk value of 2.413 Å.

Several models were evaluated, indicated by a three-digit code (*Xim*). The first digit (*X*) refers to the type of edge distortion, the second (*i*) to the magnitude of the statistical disorder, and the third (*m*) to the size of the particles. The first digit is A, B, C, D, or E and describes the edge distortion. It stands for the following: (A) There is no distortion at the edges [the Mo−

Mo distance is the same as in bulk MoS$_2$ (3.16 Å)]. (B) The Mo−Mo distance at the S-terminated edge is 2.85 Å. (C) The Mo−Mo distances at the S-terminated edge and Mo-terminated edge are 3.09 and 3.36 Å, respectively (cf. Figure 1). (D$_n$) The Mo−Mo distance at the S-terminated edge is $(3.16 + 0.04n)$ Å, with n ranging from −7 to +7. (E$_n$) The Mo−Mo distance at the S- and Mo-terminated edge is $(3.16 + 0.04n)$ Å.

The second digit is w, x, y, z, s, or t and describes the Mo disorder. It stands for the following: (w) no disorder; (x) slight disorder (r_{max} values at the edge and in the center of the particle 0.06 and 0.04 Å, respectively); (y) moderate disorder (r_{max} values at the edge and in the center of the particle 0.12 and 0.08 Å, respectively); (z) great disorder (r_{max} values at the edge and in the center of the particle 0.18 and 0.12 Å, respectively); (s) great disorder at the edge (r_{max} values at the edge and in the center of the particle 0.3 and 0.12 Å, respectively); (t) very great disorder at the edge (r_{max} values at the edge and in the center of the particle 0.4 and 0.12 Å, respectively).

The third digit is an integer which describes the "size" of the particle. The size is defined by size = (the number of the Mo atoms at an edge) − 1. The MoS$_2$ particles thus have a diameter L (in Å) of $L = 2 \times 3.16$ size = 6.32 size.

For example, model Bx4 is the model with distortion B (Mo−Mo distance at the S-terminated edge is 2.85 Å), with a slight statistical Mo disorder (x) and with 5 Mo atoms per edge. Model D$_4$z7 is the model whose Mo−Mo-1 distance at the S-terminated edge is $0.04 \times 4 = 0.16$ Å longer than that of the bulk Mo−Mo-1 distance, with a large statistical disorder (z) and with 8 Mo atoms per edge.

The distortion assumed in model B is based on the results of Byskov et al.[42] They calculated the Mo−S and Co−Mo−S bonding energy in small MoS$_2$ and Co−MoS$_2$ particles with a self-consistent density functional theory and suggested a short Mo−Mo distance of 2.85 Å at the S-terminated edge. Model C is inspired by the results of Calais et al.[41] They claimed that there are slightly longer and slightly shorter Mo−Mo distances in addition to the normal distances in the MoS$_2$ particles and that these slightly different distances cause the reduction in the CN1. Models D and E are used to investigate the effect of differences in the Mo−Mo-1 edge distance.

In the x, y, and z models, the disorder at the edges is assumed to be 50% greater than in the remainder of the particle. Even though there is no direct evidence for this assumption, it seems reasonable to assume that the edges of the MoS$_2$ particles are more irregular than the inside.

Figure 2 shows the distributions of the Mo−Mo-1 distances calculated for the models Ai7, Bi7, and Ci7 (i = w, x, y, or z). The peaks become broader with increasing disorder. In model A, the distributions are close to Gaussian for each disorder. For model B, a small peak is observed at 2.85 Å which is isolated from the main peak at 3.16 Å up to disorder z. For model C, two small peaks are observed at 3.09 and 3.36 Å in addition to the main peak at 3.16 Å for disorder w. The peak at 3.09 Å merges with the main peak starting with disorder y, and the peak at 3.36 Å starting with disorder z.

II.2. Simulation of Spectra. The EXAFS function of the MoS$_2$ particles were obtained by simulating the EXAFS function of each Mo atom in the small MoS$_2$ particles by the FEFF7 program[43] and subsequently averaging the functions of all Mo atoms in the particle. All electron paths shorter than 7.0 Å, which give an EXAFS contribution with an amplitude larger than 0.5% of the most intense contribution, including multiple scatterings up to 5 scattering atoms, were used to simulate the
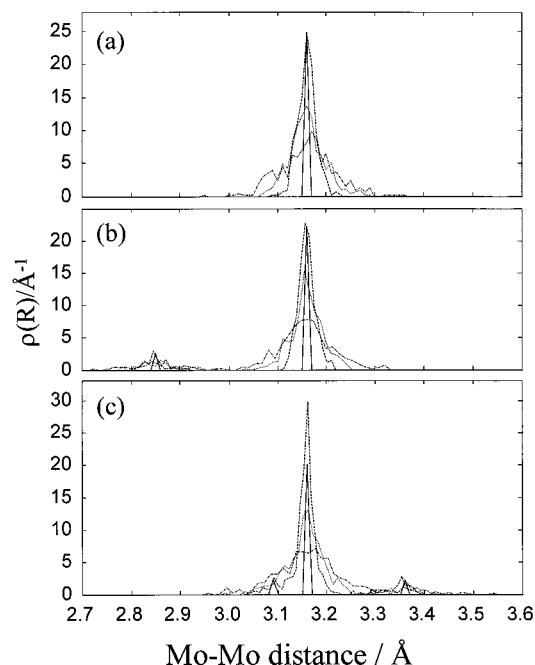
Figure 2. Distribution of the Mo−Mo-1 distances for models (a) Ai7, (b) Bi7, and (c) Ci7. The lines —, - - -, •••, and -•- represent the distributions for disorders w, x, y, and z, respectively. The magnitudes for model w were reduced by a factor of 4.

EXAFS spectra. In the simulation, the Debye temperature and the measuring temperature were assumed to be 300 and 100 K, respectively. The Debye temperature of bulk MoS_2 was reported to be 300 K.[44] As both the simulated spectra and the reference spectra were calculated with the same Debye temperature and measuring temperature, the effect of the thermal Debye−Waller factor is eliminated. Hence, the structural parameters derived by the analysis, such as CN, R, and Debye−Waller factor, are not affected by the given Debye and measuring temperatures. These values affect only the absolute amplitude of the EXAFS oscillations.

The simulated spectra were analyzed according to a conventional procedure to elucidate the structural parameters. The XDAP program[45,46] was used to analyze the simulated spectra. The simulated spectra were fitted with Mo−S and Mo−Mo distances whose phase shifts and backscattering amplitudes were also calculated by the FEFF7 code. The fit was carried out in R space, and the k range in the Fourier transformation was 3.0−19.8 Å^{-1}. The Mo−Mo-1 contribution was fitted with k^3 and k^1 weighting, the second nearest Mo−Mo contribution (Mo−Mo-2) with k^3 weighting. In k^1 weighting, the R range for the Mo−Mo-1 contribution was 1.0−4.0 Å, and the contribution was fitted together with the nearest and the second nearest Mo−S contributions (Mo−S-1 and Mo−S-2). In k^3 weighting, the R range for the fitting was 1.0−3.3 Å, and the Mo−Mo-1 contribution was fitted together with the Mo−S-1 contribution. The R range of the fitting of Mo−Mo-2 was 4.9−5.4 Å. The multiple scattering effects of the Mo−S-1 and Mo−Mo-1 contributions were subtracted from the original data to fit the Mo−Mo-2 contribution.

The interatomic distance (R), the coordination number (CN), and the difference of the Debye−Waller factor from the reference ($\Delta\sigma^2$) were treated as free parameters, while the correction of the threshold energy was fixed at 0.0 eV. The quality of the fit was estimated from the values of the variance and the goodness of the fit (ϵ_ν^2). The variance represents the residual between the observed and calculated spectrum in the
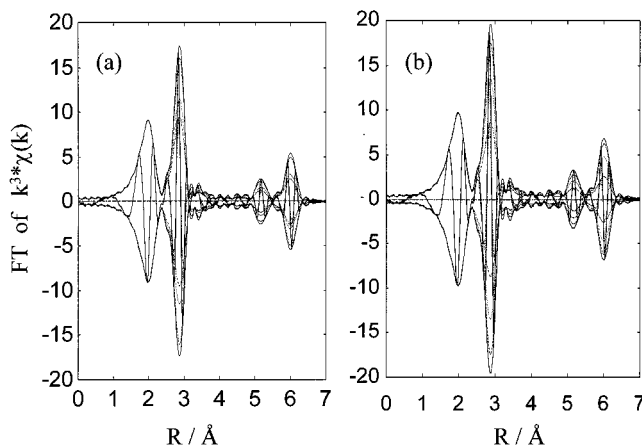

Figure 3. Absolute and imaginary parts of the Fourier-transformed k^3-weighted EXAFS functions for models Ai3 (a) and Ai7 (b). The lines —, - - -, •••, and -•- represent spectra for the disorder parameters w, x, y, and z, respectively.

fitted range and was calculated with the following formula:

$$\text{variance} = 100 \int_{R_{\min}}^{R_{\max}} k^{2n}(\text{FT}_{\text{model}} - \text{FT}_{\text{exp}})^2 \, \mathrm{d}R / \int_{R_{\min}}^{R_{\max}} k^{2n}(\text{FT}_{\text{exp}})^2 \, \mathrm{d}R$$

Variances for the real and imaginary parts of the Fourier-transformed EXAFS function were calculated separately. The ϵ_ν^2 value takes the number of free parameters into account and is used to determine whether the addition of new parameters makes sense. It was calculated with the formula

$$\epsilon_\nu^2 = (\nu/\text{NPTS}(\nu - N_{\text{free}}) \sum_{i=1}^{\text{NPTS}} ((\chi_{\text{model},i} - \chi_{\text{exp},i})/\sigma_{\text{exp}}))^2$$

where χ_{model} and χ_{exp} are the model and experimental EXAFS functions respectively, σ_{exp} is the error in the experimental data (assumed to be 0.01 for each data point), ν is the number of independent data points in the fit range, and NPTS is the actual number of data points in the fit range. Although the absolute value of ϵ_ν has no meaning, ϵ_ν enables the comparison of the goodness of fit in the same spectra and same k weighting with different parameters, a smaller ϵ_ν value meaning a better fit.

III. Results

III.1. Preliminary Simulations Using Models A−C. Figure 3 shows Fourier-transformed k^3-weighted EXAFS functions (FT of $k^3\chi(k)$) of the models Ai3 and Ai7 (i = w, x, y, and z). These models represent particles with no edge distortion, with diameters of 19.0 and 44.2 Å, respectively, and varying disorder of the Mo atoms. Peaks at 2.0 (peak 1), 2.9 (peak 2), and 5.2 Å (peak 3) are due to the Mo−S-1, Mo−Mo-1, and Mo−Mo-2 contributions, respectively. The fourth peak at 6.0 Å is mainly due to the linear Mo−Mo-3 contribution but overlaps with the multiple scattering of the Mo−Mo-1 contribution. No corrections for the phase shifts were applied in Figures 3−6 for the Fourier-transformed EXAFS functions. The second Mo−S contribution, Mo−S-2, is weak in k^3 weighting, and a shoulder at 3.1 Å is attributed to this contribution. As expected, peak 1 is independent of the disorder, because the Mo−S-1 distance has been kept at 2.413 Å, regardless of the Mo disorder. On the other hand, peaks 2−4 decreased with increasing disorder. In both MoS_2 particle sizes (sizes 3 and 7), peak 2 is higher than peak 1 for disorders w, x, and y and is lower for disorder z.
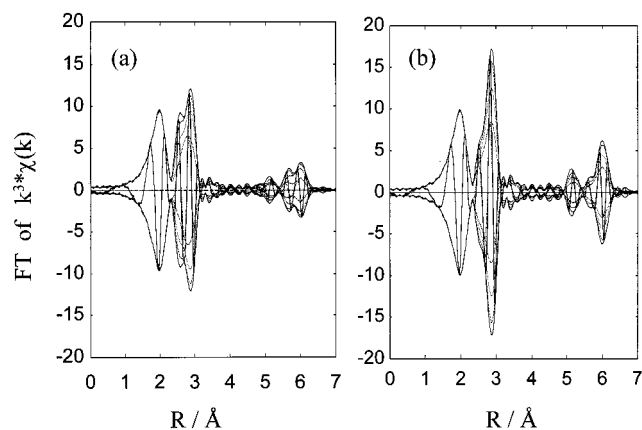
Figure 4. Absolute and imaginary parts of the Fourier-transformed k^3-weighted EXAFS functions for models Bi3 (a) and Bi7 (b). The lines —, - - -, ⋯, and -·- represent spectra for the disorder parameters w, x, y, and z, respectively.
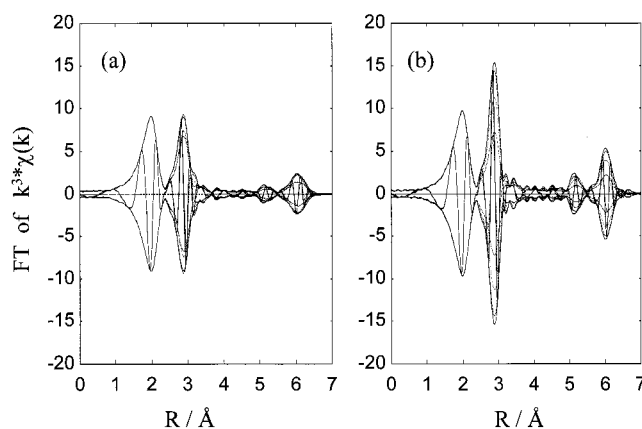

Figure 5. Absolute and imaginary parts of the Fourier-transformed k^3-weighted EXAFS functions for models Ci3 (a) and Ci7 (b). The lines —, - - -, ⋯, and -·- represent spectra for the disorder parameters w, x, y, and z, respectively.
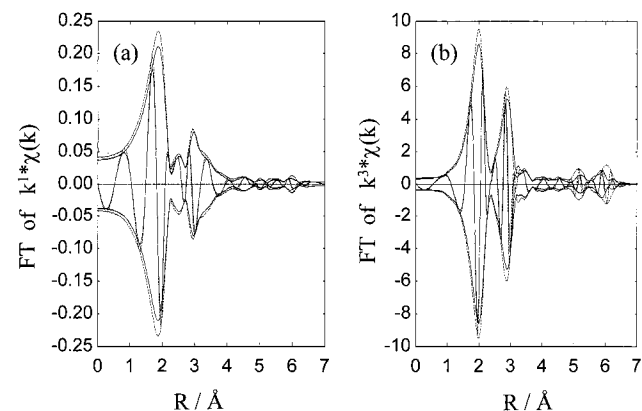

Figure 6. Fourier-transformed k^1- (a) and k^3- (b) weighted EXAFS functions for model Az2 (—) and Cz5 (- - -).

Table 1 shows structural parameters for the models Ai7 (i = w, x, y, z, s, and t) derived by curve fitting with k^3 weighting. The spectra were fitted with one Mo−S-1, one Mo−Mo-1, and one Mo−Mo-2 contribution. The quality of the fit is reasonably good and does not depend on the disorder. The Mo−Mo-1 distance is unchanged by altering the disorder, and the bond distance distribution is almost Gaussian (Figure 2a). The coordination number CN1 of the first Mo−Mo-1 contribution is not very sensitive to the magnitude of the disorder. It decreases slightly with increasing disorder (models w−z) and

TABLE 1: Results of the k^3-Weighted Curve Fittings for Models Ai7[a]

model	shell	CN	R, Å	$\Delta\sigma^2$, 10^{-4} Å²	V_{Re}	V_{Im}	goodness of fit
Aw7	Mo−S-1	5.8	2.41	0.1	0.14	0.23	0.35
	Mo−Mo-1	5.6	3.16	0.5			
	Mo−Mo-2	4.6	5.47	−0.9	0.25	1.26	0.44
Ax7	Mo−S-1	5.8	2.41	0.1	0.12	0.19	0.30
	Mo−Mo-1	5.6	3.16	4.0			
	Mo−Mo-2	4.2	5.47	0.1	0.21	2.40	0.39
Ay7	Mo−S-1	5.8	2.41	0.1	0.23	0.53	0.25
	Mo−Mo-1	5.5	3.16	12.4			
	Mo−Mo-2	4.2	5.47	8.9	0.64	3.28	0.36
Az7	Mo−S-1	5.8	2.41	0.1	0.20	0.27	0.20
	Mo−Mo-1	5.3	3.16	28.1			
	Mo−Mo-2	3.4	5.47	15.8	2.01	5.84	0.26
As7	Mo−S-1	5.7	2.41	0.0	0.19	0.28	0.17
	Mo−Mo-1	4.7	3.16	23.4			
At7	Mo−S-1	5.7	2.41	0.0	0.22	0.26	0.15
	Mo−Mo-1	4.5	3.16	24.2			

[a] V_{Re} and V_{Im} are the variances of the real and imaginary parts of the FT, respectively. The expected CN and R are 5.7 and 2.41 Å for Mo−S-1, 5.5 and 3.16 Å for Mo−Mo-1, and 5.1 and 5.47 Å for Mo−Mo-2, respectively.

TABLE 2: Results of the k^3-Weighted Curve Fittings for Models Bi7 with One Mo−Mo-1 Contribution[a]

model	shell	CN	R, Å	$\Delta\sigma^2$, 10^{-4} Å²	V_{Re}	V_{Im}	goodness of fit
Bw7	Mo−S-1	6.1	2.41	3.7	1.05	1.36	0.42
	Mo−Mo-1	5.8	3.16	4.6			
	Mo−Mo-2	3.3	5.48	−3.9	2.77	3.77	0.54
Bx7	Mo−S-1	6.1	2.41	3.4	0.87	1.15	0.33
	Mo−Mo-1	5.7	3.16	7.4			
	Mo−Mo-2	2.8	5.48	−6.3	0.46	3.75	0.44
By7	Mo−S-1	6.0	2.41	2.7	0.59	0.79	0.28
	Mo−Mo-1	5.5	3.16	13.8			
	Mo−Mo-2	3.1	5.48	3.3	0.93	3.90	0.37
Bz7	Mo−S-1	6.0	2.41	2.0	0.50	0.69	0.21
	Mo−Mo-1	5.2	3.15	26.3			
	Mo−Mo-2	3.0	5.48	16.2	2.75	7.22	0.28

[a] V_{Re} and V_{Im} are the variances of the real and imaginary parts of the FT, respectively. The expected CN and R are 5.7 and 2.41 Å for Mo−S-1, 5.5 and 3.16 Å for Mo−Mo-1, and 5.1 and 5.47 Å for Mo−Mo-2, respectively.

is close to the real value. However, the CN1 is reduced substantially if the disorder is extremely large, as in the models As7 and At7; the calculated CN1s for these models are 4.7 and 4.5, respectively (Table 1). The coordination number of the Mo−Mo-2 contribution (*CN2*) is more sensitive to the disorder, decreases with increasing disorder, and is always smaller than the actual value. The Debye−Waller factor of the Mo−Mo-1 contribution increases with increasing statistical disorder. The Debye−Waller factor is close to that of the reference in model Aw7 and much larger in model Az7. This shows that the effect of the disorder is included in the Debye−Waller factor.

Figure 4 shows the FTs of $k^3\chi(k)$ for the models Bi3 and Bi7. Peak 1 did not change, and peaks 2−4 decreased with increasing disorder, as in model A. Peak 2 is higher than peak 1 for disorders w, x, and y and lower for disorder z. A shoulder was observed on peak 2 at 2.5 Å for each disorder, which is due to the shorter Mo−Mo-1 distance at the edge as assumed in model B. The shoulder is more distinct at size 3 than size 7 and becomes smaller with increasing disorder; even for large disorder, however, two different Mo−Mo-1 contributions could be distinguished in the FTs (Figure 4). Table 2 and 3 show structural parameters for the models Bi7 derived by k^3-weighted curve fittings. The values of the goodness of fit with two Mo−

TABLE 3: Results of the k^3-Weighted Curve Fittings for Models Bi7 with Two Mo−Mo-1 Contributions[a]

model	shell	CN	R, Å	$\Delta\sigma^2$, 10^{-4} Å^2	V_{Re}	V_{Im}	goodness of fit
Bw7	Mo−S-1	5.8	2.41	0.0	0.07	0.13	0.13
	Mo−Mo-1	5.0	3.16	0.3			
	Mo−Mo-1	0.6	2.85	−0.5			
Bx7	Mo−S-1	5.8	2.41	0.0	0.08	0.12	0.25
	Mo−Mo-1	5.0	3.16	3.4			
	Mo−Mo-1	0.6	2.85	5.1			
By7	Mo−S-1	5.8	2.41	0.1	0.11	0.15	0.23
	Mo−Mo-1	4.9	3.16	10.8			
	Mo−Mo-1	0.5	2.85	13.7			
Bz7	Mo−S-1	5.7	2.41	0.0	0.12	0.18	0.16
	Mo−Mo-1	4.8	3.15	24.6			
	Mo−Mo-1	0.7	2.84	41.0			

[a] V_{Re} and V_{Im} are the variances of the real and imaginary parts of the FT, respectively. The expected CN and R are 5.7 and 2.41 Å for Mo−S-1, 4.9 and 3.16 Å for the first Mo−Mo-1, and 0.6 and 2.85 Å for the second Mo−Mo-1, respectively.

TABLE 5: Results of the k^3-Weighted Curve Fittings for Models Ci7 with Two Mo−Mo-1 Contributions[a]

model	shell	CN	R, Å	$\Delta\sigma^2$, 10^{-4} Å^2	V_{Re}	V_{Im}	goodness of fit
Cw7	Mo−S-1	5.7	2.41	−0.1	0.09	0.15	0.30
	Mo−Mo-1	4.7	3.15	3.3			
	Mo−Mo-1	0.2	3.37	−30.7			
Cx7	Mo−S-1	5.7	2.41	−0.1	0.09	0.15	0.24
	Mo−Mo-1	4.7	3.15	5.6			
	Mo−Mo-1	0.2	3.36	−28.1			
Cy7	Mo−S-1	5.7	2.41	−0.1	0.12	0.15	0.20
	Mo−Mo-1	4.6	3.15	12.8			
	Mo−Mo-1	0.1	3.38	−30.4			
Cz7	Mo−S-1	5.7	2.41	−0.2	0.18	0.22	0.19
	Mo−Mo-1	4.4	3.16	29.1			
	Mo−Mo-1	0.0	3.36	−40.3			

[a] V_{Re} and V_{Im} are the variances of the real and imaginary parts of the FT, respectively. The expected CN and R are 5.7 and 2.41 Å for Mo−S-1, 4.9 and 3.16 Å for the first Mo−Mo-1, and 0.6 and 3.36 Å for the second Mo−Mo-1, respectively.

TABLE 4: Results of the k^3-Weighted Curve Fittings for Models Ci7 with One Mo−Mo-1 Contribution[a]

model	shell	CN	R, Å	$\Delta\sigma^2$, 10^{-4} Å^2	V_{Re}	V_{Im}	goodness of fit
Cw7	Mo−S-1	5.7	2.41	−0.1	0.45	0.60	0.23
	Mo−Mo-1	4.4	3.15	−0.1			
	Mo−Mo-2	3.5	5.47	1.9	1.16	1.43	0.29
Cx7	Mo−S-1	5.7	2.41	−0.2	0.34	0.45	0.18
	Mo−Mo-1	4.3	3.15	2.0			
	Mo−Mo-2	2.8	5.47	−3.0	0.25	2.5	0.24
Cy7	Mo−S-1	5.7	2.41	−0.2	0.36	0.41	0.16
	Mo−Mo-1	4.3	3.15	9.9			
	Mo−Mo-2	2.9	5.47	4.6	0.55	3.59	0.21
Cz7	Mo−S-1	5.7	2.41	−0.3	0.24	0.29	0.12
	Mo−Mo-1	4.1	3.16	25.6			
	Mo−Mo-2	2.9	5.47	21.4	3.50	7.90	0.16

[a] V_{Re} and V_{Im} are the variances of the real and imaginary parts of the FT, respectively. The expected CN and R are 5.7 and 2.41 Å for Mo−S-1, 5.5 and 3.16 Å for Mo−Mo-1, and 5.1 and 5.47 Å for Mo−Mo-2, respectively.

TABLE 6: Results of the k^1-Weighted Curve Fittings for Models Ci7 with One Mo−Mo-1 Contribution[a]

model	shell	CN	R, Å	$\Delta\sigma^2$, 10^{-4} Å^2	V_{Re}	V_{Im}	goodness of fit
Cw7	Mo−S-1	5.6	2.41	−1.7	0.04	0.13	0.09
	Mo−Mo-1	4.1	3.15	2.4			
	Mo−S-2	5.3	3.98	29.4			
Cx7	Mo−S-1	5.6	2.41	−1.8	0.03	0.14	0.07
	Mo−Mo-1	4.2	3.15	0.9			
	Mo−S-2	4.6	3.98	18.2			
Cy7	Mo−S-1	5.6	2.41	−1.7	0.03	0.13	0.06
	Mo−Mo-1	4.1	3.15	7.9			
	Mo−S-2	4.5	3.98	33.6			
Cz7	Mo−S-1	5.7	2.41	−1.4	0.02	0.12	0.05
	Mo−Mo-1	4.2	3.16	26.7			
	Mo−S-2	4.8	3.98	65.7			

[a] V_{Re} and V_{Im} are the variances of the real and imaginary parts of the FT, respectively. The expected CN and R are 5.7 and 2.41 Å for Mo−S-1, 5.5 and 3.16 Å for Mo−Mo-1, and 4.7 and 3.92 Å for Mo−S-2, respectively.

Mo-1 contributions are smaller than those with one Mo−Mo-1 contribution for every disorder, indicating that the fitting with two Mo−Mo-1 contributions is preferable to that with one Mo−Mo-1 contribution. The calculated CN1 and Mo−Mo-1 distance agree with the actual values if the fitting was carried out with two Mo−Mo-1 contributions. In real catalytic MoS$_2$ systems only one Mo−Mo-1 contribution has ever been observed; thus, model B does not reproduce the observed data. This must be caused by too great a difference between the edge and bulk Mo−Mo-1 distances.

Figure 5 shows the FTs of $k^3\chi(k)$ for the models Ci3 and Ci7. Peak 1 did not change and peaks 2−4 decreased with increasing disorder, as in models A and B. The position of peak 3 shifts to a longer distance with increasing disorder. The intensity of peak 2 for size 7 is greater than that of peak 1 for disorders w, x, and y and smaller for disorder z. The shape of peak 2 in model C is quite similar to that in model A. The intensity of peak 2 in model C is smaller than that in model A at sizes 3 and 7. However, if the size is not known, it is almost impossible to distinguish models A and C, both in k^3 or in k^1 weighting. For example, the EXAFS functions for models Az2 and Cz5 are very similar in k^3 as well as k^1 weighting in the 0−4 Å range, as shown in Figure 6.

Tables 4−6 show structural parameters obtained for models Ci7 by k^3- and k^1-weighted curve fittings. The bulk and edge Mo−Mo-1 contributions are distinct (fitting converged), but the

shorter Mo−Mo-1 contribution could not be distinguished from the bulk Mo−Mo-1 contribution. The curve fittings give correct Mo−Mo-1 distances, but the CN1 is underestimated for the k^1- as well as for the k^3-weighted fitting. The variance decreases substantially by including the longer Mo−Mo-1 contribution. The goodness of fit, however, does not improve in any magnitude of disorder (or even gets worse) by adding the longer Mo−Mo-1 contribution, which means that the inclusion of the longer Mo−Mo distance does not make sense mathematically. In k^1 weighting, the fitting process did not converge when the fitting was carried out with two Mo−Mo-1 contributions. The degree of disorder does not affect the CN1 very much, as shown in Tables 4−6. The Debye−Waller factor of Mo−Mo-1 increases with increasing disorder; disorder is absorbed in the Debye−Waller factor, as in models A and B.

The variances for the real and imaginary parts (V_{Re} and V_{Im}) in the k^3-weighted fitting with one Mo−Mo-1 shell for models Aw7, Az7, Cw7, and Cz7 are (0.14, 0.23), (0.20, 0.27), (0.45, 0.60), and (0.24, 0.29), respectively (Tables 1 and 4). The variances of Cw7 are larger than those of Aw7, while the variances of Cz7 are comparable to those of Az7. This demonstrates that the edge distortion deteriorates the quality of the fit in the case of no disorder and that it does not affect the quality in the case of a large disorder. Because the Mo−Mo coordination number CN1 is underestimated in model C, a distortion can reduce the CN1 without being noticed in the fitting procedure.
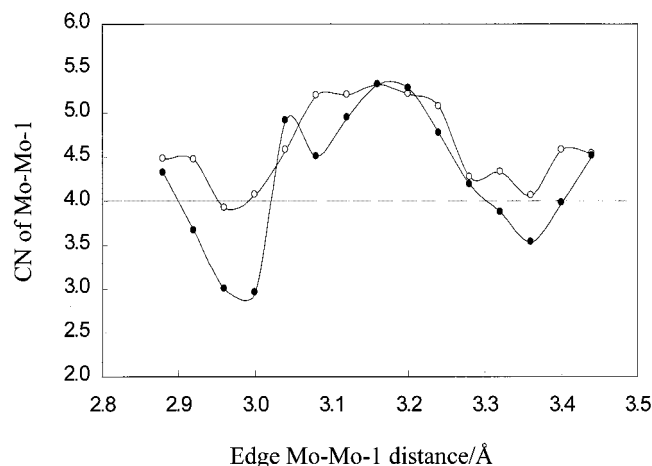
Why EXAFS Underestimated the Size of MoS$_2$ Particles

J. Phys. Chem. B, Vol. 102, No. 43, 1998 **8431**

Figure 7. *CN* of Mo−Mo-1 for models D$_n$z7 (●) and E$_n$z7 (○) derived by a conventional EXAFS analysis as a function of the average edge Mo−Mo-1 distance. The fitting was carried out with one Mo−Mo-1 shell.

The following conclusions can be drawn from the models and will be discussed in more detail in the Discussion: (1) Disorder z is the most probable disorder, because only this disorder reproduces the observed lower intensity of peak 2 than of peak 1. (2) k^3 weighting is better than k^1 weighting. The curve fitting with k^3 weighting converged, while that with k^1 did not converge for model C in the fitting with two Mo−Mo-1 shells. (3) The difference between the edge and bulk Mo−Mo-1 distances should be smaller than 0.3 Å, because only one Mo−Mo-1 contribution is observed and model B cannot reproduce this. (4) The Mo−Mo-2 contribution is smeared by the disorder and distortion. The diameter of the MoS$_2$ slabs cannot be estimated from the *CN*2 contribution.

III.2. Most Probable Models. In a TEM and EXAFS study of small MoS$_2$ particles, the diameters of the MoS$_2$ slabs and their distribution were elucidated by TEM.[41] The average size (number of Mo atoms at the edge minus one) was found to be seven. The Mo−Mo-1 coordination number revealed by EXAFS analysis was 4.0. The EXAFS spectrum of these well-characterized small MoS$_2$ particles can be used as a standard to evaluate our models. In this section, we concentrate on the models D$_n$z7 and E$_n$z7 with disorder z and size 7 as well as on the Mo−Mo-1 contribution and fitting in k^3 weighting. This strategy is suggested by the results reported in section III.1.

The criteria for evaluating the models are CN1 should be close to 4.0, the simulated spectra should be fitted with one Mo−Mo-1 contribution, and the variances should be smaller than those of the fitting for model Cz7 with one Mo−Mo-1 contribution. The sum of variances for the real and imaginary parts ($V_{re} + V_{Im}$) will be used for the evaluation (the value for model Cz7 is 0.53).

Figures 7 and 8 show CN1 and $V_{re} + V_{Im}$ as a function of the Mo−Mo-1 edge distance, respectively. The CN1 is too high if the difference between the Mo−Mo-1 distances at the edge and in the bulk is smaller than 0.1 Å in both models. A simulated spectrum with a shorter Mo−Mo-1 edge distance than 3.06 Å cannot be fitted by one Mo−Mo-1 contribution and gives a large $V_{re} + V_{Im}$ (Figure 8). Model C is already a good model, and only a limited number of models in the D and E series are better than model C. Models D$_{−5}$ (with edge Mo−Mo-1 distance of 2.96 Å), D$_3$ (3.28 Å), and D$_4$ and E$_4$ (3.32 Å) and models D$_5$ and E$_5$ (3.36 Å) satisfy the criteria more or less.

For further evaluation, the EXAFS of smaller sized (size = 4−6) particles were fitted, and their $V_{re} + V_{Im}$ values are shown
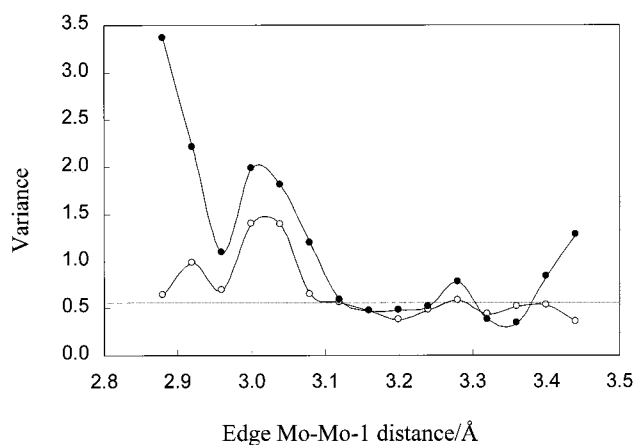

Figure 8. Variance (sum of variances for the real part and the imaginary part) of curve fitting of the Mo−Mo-1 contribution for models D$_n$z7 (●) and E$_n$z7 (○) as a function of the average edge Mo−Mo-1 distance. The fitting was carried out with one Mo−Mo-1 shell.
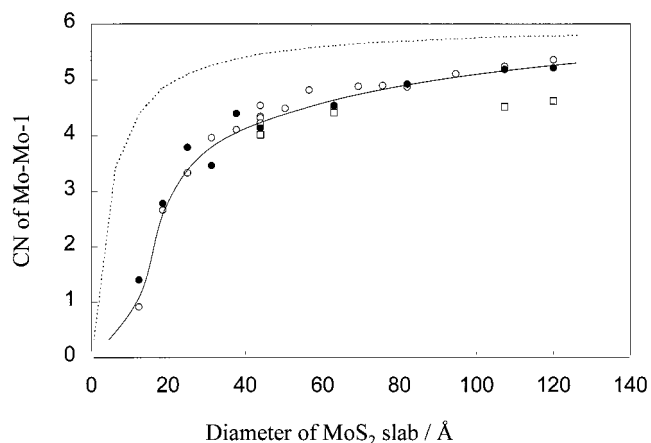

Figure 9. Calculated average *CN* of Mo−Mo-1 by EXAFS analysis (—) as a function of the diameter of the MoS$_2$ particles for models D$_4$z (●) and Cz (○). □ represents the observed values for particles whose sizes were determined by TEM in ref 41. The dotted line shows the CN1 value for MoS$_2$ slabs with the Mo and S atoms rigidly located at the ideal bulk structure positions.

in Table 7S (available as Supporting Information). Only the models D$_3$, D$_4$, D$_5$, and E$_5$ can be fitted with one Mo−Mo-1 shell at smaller sizes, but the CN1 calculated for E$_5$ is too small (*CN* = 3.53). The quality of the curve fitting for models D$_4$z is good for all sizes and insensitive to a small deviation of the edge Mo−Mo-1 distance, because models D$_3$ and D$_5$ also satisfy the criteria.

As expected, distortion of the Mo-terminated edge instead of the S-terminated edge gives identical spectra, and it is impossible to determine which edge (either the S or Mo-terminated edge) is distorted.

The above results indicate that the models Cz and D$_4$z are the most probable models. Therefore, the CN1s were calculated for these models with sizes in the range of 2−19. The results are shown in Figure 9 together with the experimental data.[41] The calculated CN1s for the models Cz and D$_4$z are close to those observed at sizes 7 and 10 (*L* = 44.2 and 63.2 Å, respectively) but are larger than the experimental values at sizes 17 and 19 (*L* = 107.4 and 121.0 Å, respectively). In these cases, the CN1 hardly changes when a particle size distribution is taken into account, because the CN1 increases almost linearly with increasing diameter above 40 Å. The CN1s calculated for the models Cz and D$_4$z are similar, which means that a slight difference in the edge distortion does not affect the CN1.

The EXAFS spectra for the model D_4z7 were simulated four times to estimate the effect of the random positioning of the Mo atoms. The standard deviation for the calculated CN1 was estimated to be 0.2.

The CN1 of rigid MoS_2 slabs with the same structure as bulk MoS_2 increases rapidly with increasing slab diameter between 0 and 10 Å and only slowly above 40 Å. The CN1 of our models, on the other hand, increases rapidly with increasing diameter in the 10−30 Å range and gradually above 40 Å. The difference between the idealized and model CN1 is very large below slab diameters of 20 Å and becomes smaller with increasing slab diameter.

IV. Discussion

IV.1. Effect of Disorder. The magnitude of the statistical disorder can be estimated by comparing the simulations performed with the models A−C and the experimental data. Up to moderate disorder (w, x, or y), the peak intensity of the Mo−Mo-1 contribution in the FT of $k^3\chi(k)$ (peak 2) is higher than that of the Mo−S-1 contribution (peak 1) for any distortion (model A, B, or C). Even in model Aw1, which describes extremely small hexagonal Mo_7S_{12} particles without any distortion and disorder, peak 2 is larger than peak 1. Peak 2 is always smaller than peak 1, on the other hand, for disorder z at all distortions and any size up to 10 and comparable to peak 1 between size 10 and 19. The disorder z satisfies the criterion that the peak intensity of the Mo−Mo-1 contribution is smaller than that of the Mo−S-1 contribution in the Fourier-transformed k^3-weighted EXAFS function. Hence, the disorder of the Mo atomic positions in real samples may at least be comparable to the statistical disorder z.

The peak height is affected not only by the statistical Debye−Waller factor but also by the thermal Debye−Waller factor, the Debye temperature (Θ_D). The Θ_D of small particles could be different from bulk MoS_2, and this difference could affect the peak height. Hence, it could be dangerous, in principle, to estimate the degree of disorder by a simple comparison of the peak height in the FT of $k^3\chi(k)$. However, the Θ_D of the small particles is unknow and we have to take the bulk value to approximate the real value. As the estimation of the degree of disorder is qualitative in this study, the difference in Θ_D should not be a big problem in the estimation.

As shown in Tables 2−6, the effect of the disorder is almost completely included by a change in the Debye−Waller factor, and the CN1 decreases only slightly with increasing disorder up to disorder z. For model C, one of the probable models, the CN1 decreases from 4.4 at disorder w to 4.1 at z. This change is hardly significant compared to the experimental result, because the standard deviation in the CN1 is estimated to be 0.2 from the model D_4z7 as shown in Figure 9. This is reasonable, because the distribution of Mo−Mo-1 distances is broadened symmetrically as shown in Figure 2. In particular, the distribution for model A is close to Gaussian.

The CN1 can be reduced from its real value by an extremely large edge disorder as demonstrated by models As7 and At7 (Table 1). The calculated CN1s for models As and At are 4.7 and 4.5, respectively, substantially lower than the value of 5.5 predicted for an ideal rigid MoS_2 particle of size 7. Startsev and Kochubei claimed that the reduction of the CN1 could be attributed to a large edge disorder.[18] They proposed that the Deby−Waller factor for the edge Mo−Mo-1 contribution is much larger than that for the bulk and that the edge Mo−Mo-1 contribution cannot be detected by EXAFS. The results of our simulations show, however, that the CN1 does not decrease

rapidly enough with increasing edge disorder to become invisible. The CN1 is still substantially larger (4.5) than the observed CN1 (4.0) at an unusually large edge disorder (r_{max} of 0.4 Å) for model At. Thus, the suggestion of Startsev and Kochubei can be excluded.

IV.2. Effect of Edge Distortion. A quicker reduction of the CN1 can be achieved, on the other hand, with a small distortion of the atomic positions of the Mo edge atoms. The magnitude of the distortion does not have to be larger than 0.2 Å to explain the reduction in intensity of CN1, as described in section III.2. In contrast to the disorder, the magnitude of the edge distortion cannot be determined by EXAFS if the slab diameter is unknown. A small particle without edge distortion gives a similar spectrum as a large particle with distortion if the disorder is large. For example, the spectra of the models Az2 and Cz5 are difficult to distinguish in k^3 as well as in k^1 weighting, as shown in Figure 6. A curve fitting taking higher cumulants into account, the so-called ratio method, is not applicable either, because the Mo−Mo-1 contribution overlaps with the Mo−S-1 and Mo−S-2 contributions and the ratio method requires isolated contributions.[47,48] Furthermore, the Mo−Mo-1 distance distribution produced by the edge distortion cannot be reproduced exactly by a cumulant expansion.

A substantial difference, however, was observed in the region of higher shells (5−7 Å) in the k^3-weighted spectra, as shown in Figure 6b. The intensity of peak 3 in model Az2 is substantially smaller than that in model Cz5, and it looks as if this peak could be used for particle size determination. However, the higher shell contribution changes in a complicated manner with a change in distortion and disorder. In addition, Mo−Mo contributions between MoS_2 layers, which are not taken into account in this simulation, and the Mo−Mo-2 contribution in real samples become superimposed. Much more work is therefore required to find out if the diameter of the MoS_2 slab and the magnitude of the distortion can be determined simultaneously from the higher shell region.

The comparison of the simulations with the experimental results[3,9−20,41] shows that small MoS_2 particles contain a substantial amount of distortion and disorder. The Mo−Mo-1 contribution is reduced in intensity without any further indication of a distortion and is very close to the Mo−Mo-1 contribution of undistorted smaller MoS_2 particles. One important conclusion of our simulations is that the edge Mo−Mo-1 distance should be longer than that of the bulk by about 0.16 Å. Models with shorter Mo−Mo-1 distances at the edge than in the bulk cannot reproduce the observed data, although a density-functional theory (DFT) calculation suggested a shorter Mo−Mo-1 distance at the S-terminated edges.[42] The DFT calculation was carried out for a narrow strip of MoS_2 (about 6 Å in width), and such a MoS_2 model particle is quite different from small MoS_2 particles in real catalysts.

IV.3. Particle Size Estimation. Although it is impossible to determine the diameter of the MoS_2 particles and the magnitude of the distortion of an unknown sample by one EXAFS experiment, one could determine the diameter of the slabs if the magnitude of the distortion could be obtained from well-defined or well-characterized samples of known diameter. If the MoS_2 particles in an unknown sample have the same edge distortion as that in well-characterized samples, then this distortion can be used to determine the diameter of unknown samples. We have used the spectrum of the sample with size 7 in ref 41 as a reference EXAFS spectrum to evaluate the models, because the slab diameter of this sample is well characterized (44 Å in diameter) and has a narrow distribution.

The observed CN1 was 4.0 ± 0.2. Hence, we will evaluate our models by requiring that CN1 is close to 4.0 and that it is possible to fit the spectrum with one Mo–Mo-1 contribution.

The CN1s for the probable models Cz and D₄z are presented as a function of slab diameter in Figure 9 together with experimental data.[41] The standard deviation for CN1 for model D₄z7 was calculated to be 0.2, and the error in the experimentally obtained CN1 is 0.2.[41] Thus, the calculated and experimental CN1s for relatively small MoS₂ particles ($L = 44$ and 63 Å) agree within the error limits. For large particles, however, the calculated CN1s are substantially larger than the observed values. This disagreement does not disappear when a distribution of the slab diameter is taken into account. The average CN1s are calculated to be 4.2 and 5.2 for the samples with diameters of 44 and 63 Å, respectively, when the distributions of diameters in these samples, as described in ref 41, are used together with Figure 9.

The disagreement can be explained by an irregularity of the particle shape and/or a distortion at borders of domains. Small MoS₂ particles on catalyst supports are not regular hexagons, while the curve in Figure 9 is calculated for regular hexagons. CN1s for irregular hexagons are somewhat smaller than those for regular hexagons. Another possibility is that the somewhat larger MoS₂ particles may consist of several domains and that the borders of the domains are distorted like the edges of the particle. Such borders reduce the CN1, while they cannot be observed by TEM. It is also possible that the estimated disorder z is still smaller than the actual disorder. For a large slab, the effect of the edge distortion becomes smaller, and the disorder effect becomes dominant. Even though the magnitude of the disorder has a minor effect on CN1, CN1 decreases with increasing disorder as shown in Table 1. The particle size estimated by Figure 9 is reasonably close to the real value for smaller MoS₂ particles but underestimates the size of large particles.

An important result of the present simulation is that the simulated CN1 drops sharply below size 5 ($L = 30$ Å) as shown in Figure 9. In ref 41 only data for $L \geq = 44$ Å are given, and these experimental data suggest that the CN1 is reduced by a factor of about 0.7 to 0.8 above size 7 ($L = 44$ Å). In addition, our model suggests that the difference between the calculated CN1 and the actual CN1 becomes larger with decreasing particle size and that the calculated CN1 is less than half of the actual CN1 for $L \leq 20$ Å.

Although the degree of distortion and the slab diameter cannot be determined simultaneously, it is reasonable to assume that supported small MoS₂ particles possess a similar statistical disorder and edge distortion to the relatively larger unsupported MoS₂ particles. It is unlikely that the Mo atoms of smaller MoS₂ particles occupy regular positions, while the Mo atoms of unsupported MoS₂ particles are quite distorted and disordered. Rather, the degree of disorder and distortion is expected to become larger with decreasing slab diameter, which also results in the underestimation of the diameter in Figure 9.

IV.4. Comparison of EXAFS and TEM Results. The diameter of supported MoS₂ and CoMoS₂ particles on several supports was investigated by means of EXAFS[12,15,17–19] (Table 8S, available as Supporting Information). The observed CN1s are widely distributed in a range of 2.4–5.2, but the CN1 of similar samples (the same support, the same promoter, and a similar Mo loading) are very close. EXAFS of MoS₂/Al₂O₃ and CoMoS₂/Al₂O₃, with a Mo loading of about 7–8 wt %, were measured by three groups, and the CN1s for both catalysts scatter around 3. The slab diameters are estimated to be 20–

30 Å and less than 10 Å from the solid and dotted lines in Figure 9, respectively.

On the other hand, the diameter and the number of slabs in a stack of several MoS₂ samples were also studied by means of TEM[15,24,26–28,31] (Table 9S, available as Supporting Information). The average slab diameter was estimated to be 20–40 Å. Hence, the EXAFS and TEM results basically agree with each other if the solid line in Figure 9 is used to estimate the diameter. The dotted line in Figure 9 obviously underestimates the diameter, which demonstrates that the main reason for the contradiction between EXAFS and TEM results is the assumption of a regular crystal when the slab diameter is calculated from EXAFS data.

Even when Figure 9 is applied, however, the average diameter derived by EXAFS (20–30 Å) still seems to be smaller than that determined by TEM (30–40 Å). There are two possibilities to explain the discrepancy. One possibility is a finite resolution of TEM. MoS₂ particles with a diameter smaller than 20 Å cannot be observed very well by TEM.[31] Hence, TEM tends to overestimate the particle size. The other possibility is that the distribution of the diameters causes the discrepancy. We calculated the average CN1 by taking the particle size distribution into account to determine the reason for the discrepancy. Louwers et al. measured EXAFS and TEM of the same CoMoS₂/Al₂O₃ sample and also measured the distribution using TEM.[15] The average CN1 can be calculated from Figure 9 when the distribution observed by TEM is taken into account. In this way, the average CN1 is calculated to be 3.1, which is in perfect agreement with the value of 2.9–3.2 revealed by EXAFS. This result suggests that TEM and EXAFS results agree well when Figure 9 is used to estimate the particle size and that the proportion of the small particles which are unobservable by TEM is not so large that it affects the average particle size very much.

Payen et al. published a comprehensive study on the particle size of supported MoS₂ particles.[32] They took TEM photographs of 13 kinds of supported MoS₂ particles and investigated their particle size distributions. The calculated CN1s are listed in Table 9S (available as Supporting Information). The calculated values are between 3 and 4, more or less in agreement with the EXAFS data. The slight difference in the average diameter can be explained by the nonlinearity of the function relating the diameter to the observed CN1 by EXAFS. CN1 increases quickly with particle size below a diameter of 20 Å, as shown in Figure 9, but the rate of increase becomes slower at larger diameters. As a result, the fraction of small MoS₂ particles with a diameter less than 20 Å reduces the CN1 detected by EXAFS and causes an underestimation of the average diameter.

The good agreement between the slab diameters obtained by EXAFS and TEM, when the distribution of particle sizes is taken into account, implies that the function in Figure 9 is useful for estimating the slab diameter of supported MoS₂ particles.

The distortion of the MoS₂ edges and the disorder of the Mo positions explains not only the discrepancy between EXAFS and TEM but also discrepancies in the EXAFS explanations themselves. From the Mo–Mo-1 coordination number of 4, a particle diameter of 10 Å was derived, assuming that all MoS₂ particles are ideal and rigidly structured (Figure 9, dotted curve). Nevertheless, at the same time quite intense Mo–Mo-2 and Mo–Mo-3 contributions were observed, and the Mo–S-1 and Mo–Mo-1 coordination distances were found to be equal to those in bulk MoS₂. These observations do not seem to be in accordance with the presence of 10 Å MoS₂ particles. For such

small particles, one expects much smaller Mo−Mo-2 and Mo−Mo-3 intensities and coordination distances different from those in bulk MoS_2. The present work explains this discrepancy. When distortions and disorder are taken into account in the analysis of the observed Mo−Mo-1 coordination number (Figure 9, solid curve), then the size of the MoS_2 particles is much larger than expected from the dotted curve in Figure 9. As a consequence, only a minority of the Mo atoms (and not a substantial part) is located at the edges. The majority of the Mo atoms is in the center of the MoS_2 particles, and these atoms have normal MoS_2-type coordination distances and long range order.

IV.5. Other Techniques To Simulate Disorder Systems. The reverse Monte Carlo (RMC) simulation[49−54] is sometimes used to interpret data of large disordered systems such as glasses. In the RMC method, atomic positions are optimized by a random walk with several conditions to reproduce experimental data such as neutron and X-ray diffraction. There are two technical difficulties, however, to apply the technique to our system. One difficulty is the treatment of edges. The RMC method is usually used for bulk systems and not for small clusters and particles because the treatment of the interface can be difficult in this method. Another difficulty is that the data given in ref 41 are limited to apply this technique.

A molecular dynamic (MD) simulation could also be applicable. Clausen et al. applied the method to simulate the structure of small Cu particles.[34,35,55] They calculated the EXAFS function of a simulated structure and found that the pair distribution function is asymmetrical even at low temperature, which causes an underestimation of the Cu−Cu coordination number. The interatomic potential should be well estimated to apply this technique, which is not very easy in some cases. Nevertheless, the method could be useful for a further study of the present system, such as temperature dependence of the structure. Further study is required to fully understand the structure and dynamic behavior of small MoS_2 particles.

V. Conclusions

The observed EXAFS data of well-characterized small MoS_2 particles can be simulated with a model in which it is assumed that the MoS_2 particles are highly distorted and disordered. In the most probable simulation model, the nearest neighbor Mo−Mo distances on the S- or Mo-terminated edges are greater by about 0.16 Å than those in bulk MoS_2. Models with shorter edge Mo−Mo-1 distances than in the bulk cannot reproduce the observed data.

The reason that EXAFS underestimated the diameter of the MoS_2 particles is that the nearest neighbor Mo−Mo coordination number was interpreted for ordered MoS_2 particles, while the MoS_2 particles are highly distorted and disordered. Besides the distortions and disorder discussed in this work, other effects such as curvature of the slabs, defects, and site disorder may play a role as well. Because of all these possible distortions and disorders, it is difficult to determine the MoS_2 slab diameter and the magnitude of the distortion simultaneously from EXAFS data only.

A model was developed which can be used to estimate the particle size of small MoS_2 particles. With this model, the particle size estimated by EXAFS and TEM was the same.

Supporting Information Available: Table 7S (variances for models $D_n z$ and $E_n z$ with sizes $m = 4−6$), Table 8S (EXAFS data on supported MoS_2 particles), and Table 9S (TEM data on supported MoS_2 particles (4 pages)). Ordering information is given on any current masthead page.

References and Notes

(1) Ratnasamy, P.; Sivasanker, S. *Catal. Rev. Sci. Eng.* **1980**, *22*, 401.
(2) Grange, P. *Catal. Rev. Sci. Eng.* **1980**, *21*, 135.
(3) Topsøe, H.; Clausen, B. S. *Catal. Rev. Sci. Eng.* **1984**, *26*, 395.
(4) Prins, R.; de Beer, V. H. J.; Somorjai, G. A. *Catal. Rev. Sci. Eng.* **1989**, *31*, 1.
(5) Breysse, M.; Portefaix, J. L.; Vrinat, M. *Catal. Today* **1991**, *10*, 489.
(6) Delmon, B. *Catal. Lett.* **1993**, *22*, 1.
(7) Chianelli, R. R.; Daage, M.; Ledoux, M. J. *Adv. Catal.* **1994**, *40*, 177.
(8) Startsev, A. N. *Catal. Rev. Sci. Eng.* **1995**, *37*, 353.
(9) Clausen, B. S.; Topsøe, H.; Candia, R.; Villadsen, J.; Lengeler, B.; Als-Nielsen, J.; Christiansen, F. *J. Phys. Chem.* **1981**, *85*, 3868.
(10) Candia, R.; Clausen, B. S.; Bartholdy, J.; Topsøe, N.-Y.; Lengeler, B.; Topsøe, H. Proceedings of the 8th International Congress on Catalysis, Berlin, 1984; Verlag Chemie: Weinheim, Germany, 1984; Vol. 2, p 375.
(11) Chiu, N.-S.; Bauer, S. H.; Johnson, M. F. L. *J. Catal.* **1986**, *98*, 32.
(12) Bouwens, S. M. A. M.; Prins, R.; de Beer, V. H. J.; Koningsberger, D. C. *J. Phys. Chem.* **1990**, *94*, 3711.
(13) Bouwens, S. M. A. M.; van Veen, J. A. R.; Koningsberger, D. C.; de Beer, V. H. J.; Prins, R. *J. Phys. Chem.* **1991**, *95*, 123.
(14) Louwers, S. P. A.; Prins, R. *J. Catal.* **1992**, *133*, 94.
(15) Louwers, S. P. A.; Crajé, M. W. J.; van der Kraan, A. M.; Geantet, C.; Prins, R. *J. Catal.* **1993**, *144*, 579.
(16) Shimada, H.; Matsubayashi, N.; Saito, T.; Yoshimura, Y.; Imamura, M.; Kameoka, T.; Nishijima, A. *Catal. Lett.* **1993**, *20*, 81.
(17) Bouwens, S. M. A. M.; van Zon, F. B. M.; van Dijk, M. P.; van der Kraan, A. M.; de Beer, V. H. J.; van Veen, J. A. R.; Koningsberger, D. C. *J. Catal.* **1994**, *146*, 375.
(18) Startsev, A. N.; Kochubei, D. I. *Kinet. Catal.* **1994**, *35*, 543.
(19) Leliveld, R. G.; van Dillen, A. J.; Geus, J. W.; Koningsberger, D. C. *J. Catal.* **1997**, *165*, 184.
(20) Clausen, B. S.; Topsøe, H. *X-ray absorption fine structure for catalysts and surfaces;* Iwasawa, Y., Ed.; Series on Synchrotron Radiation Techniques and Applications Vol. 2; World Scientific: Singapore, 1996; p 235.
(21) Pollack, S. S.; Sanders, J. V.; Tischar, R. E. *Appl. Catal.* **1983**, *8*, 383.
(22) Zaikovskii, V. I.; Plyasova, L. M.; Burmistrov, V. A.; Startsev, A. N.; Yermakov, Yu. I. *Appl. Catal.* **1984**, *11*, 15.
(23) Delannay, F. *Appl. Catal.* **1985**, *16*, 135.
(24) Hayden, T. F.; Dumesic, J. A. *J. Catal.* **1987**, *103*, 366.
(25) Mauchausse, C.; Mozzanega, H.; Turlier, P.; Dalmon, J. A. *Proceedings of the 9th International Congress on Catalysis, Calgary, 1988*; Phillips, M. J., Ternan, M., Eds.; The Chemical Institute of Canada: Ottawa, 1998; Vol. 2, p 775.
(26) Kemp, R. A.; Ryan, R. C.; Smegal, J. A. *Proceedings of the 9th International Congress on Catalysis, Calgary, 1988*; Phillips, M. J., Ternan, M., Eds.; The Chemical Institute of Canada: Ottawa, 1998; Vol. 2, p 128.
(27) Ramirez, J.; Fuentes, S.; Diaz, G.; Vrinat, M.; Breysse, M.; Lacroix, M. *Appl. Catal.* **1989**, *52*, 211.
(28) Pratt, K. C.; Sanders, J. V.; Christov, V. *J. Catal.* **1990**, *124*, 416.
(29) Hamon, D.; Vrinat, M.; Breysse, M.; Durand, B.; Beauchesne, F.; des Courieres, T. *Bull. Soc. Chim. Belg.* **1991**, *100*, 933.
(30) Srinivasan, S.; Datye, A. K.; Peden, C. H. F. *J. Catal.* **1992**, *137*, 513.
(31) Eijsbouts, S.; Heinerman, J. J. L.; Elzerman, H. J. W. *Appl. Catal.* **1993**, *105*, 53.
(32) Payen, E.; Hubaut, R.; Kasztelan, S.; Poulet, O.; Grimblot, J. *J. Catal.* **1994**, *147*, 123.
(33) Stockmann, R. M.; Zandbergen, H. W.; van Langeveld, A. D.; Moulijn, J. A. *J. Mol. Catal.* **1995**, *102*, 147.
(34) Crozier, E. D.; Rehr, J. J.; Ingalls, R. *X-ray Absorption; Principles, Applications, Techniques of EXAFS, SEXAFS, and XANES*; Koningsberger, D. C., Prins, R., Eds.; Wiley: New York, 1988; p 373.
(35) Clausen, B. S.; Gråbæk, L.; Topsøe, H.; Hansen, L. B.; Stoltze, P.; Nørskov, J. K.; Nielsen, O. H. *J. Catal.* **1993**, *141*, 368.
(36) Clausen, B. S.; Topsøe, H.; Hansen, L. B.; Stoltze, P.; Nørskov, J. K. *Catal. Today* **1994**, *21*, 49.
(37) Dabla, G.; Formasini, P. *J. Synchrotron Rad.* **1997**, *4*, 243.
(38) Rochenberger, J.; Tröger, L.; Kornowski, A.; Vossmeyer, T.; Eychmüller, A.; Feldhaus, J.; Weller, H. *J. Phys. Chem.* **1997**, *101*, 2691.
(39) Marcus, M. A.; Flood, W.; Steigerwald, M.; Brus, L.; Bawendi, M. *J. Phys. Chem.* **1991**, *95*, 1572.
(40) Marcus, M. A.; Brus, L. E.; Murray, C.; Bawendi, M. G.; Prasad, A.; Alivisatos, A. P. *Nanostruct. Mater.* **1992**, *1*, 323.

Why EXAFS Underestimated the Size of MoS$_2$ Particles

J. Phys. Chem. B, Vol. 102, No. 43, 1998 **8435**

(41) Calais, C.; Matsubayashi, N.; Geantet, C.; Yoshimura, Y.; Shimada, H.; Nishijima, A.; Lacroix, M.; Breysse, M. *J. Catal.* **1998**, *174*, 130.

(42) Byskov, L. S.; Hammer, B.; Nørskov, J. K.; Clausen, B. S.; Topsøe, H. *Catal. Lett.*, **1997**, *47*, 177.

(43) Zabinsky, S. I.; Rehr, J. J.; Ankudinov, A.; Albers, R. C.; Eller, M. J. *Phys. Rev. B* **1995**, *52*, 2995.

(44) Volovik, L. S.; Bayhenova, L. N.; Bolger, A. S.; Klochkov, L. A.; Drozdova, S. V.; Primachenko, V. F.; Timofeeva, I. I. *Inorg. Mater. (USSR)* **1979**, *15*, 500.

(45) van Zon, J. B. A. D.; Koningsberger, D. C.; van't Blik, H. F. J.; Sayers, D. E. *J. Chem. Phys.* **1985**, *82*, 5742.

(46) Kirlin, P. S.; van Zon, F. B. M.; Koningsberger, D. C.; Gates, B. C. *J. Phys. Chem.* **1990**, *94*, 8439.

(47) Bunker, G. *Nucl. Instrum. Methods* **1983**, *207*, 437.

(48) Tranquada, J. M.; Ingalls, R. L. *Phys. Rev. B* **1983**, *28*, 3520.

(49) McGreevy, R. L.; Pusztai, L. *Mol. Simul.* **1988**, *1*, 359.

(50) Keen, D. A.; McGreevy, R. L. *Nature* **1990**, *344*, 423.

(51) Wicks, J.; Börjesson, L.; McGreevy, R. L.; Howells, W. S.; Bushnell-Wye, G. *Phys. Rev. Lett.* **1995**, *74*, 726.

(52) Swenson, J.; Boerjesson, L.; Howells, W. S. *Phys. Scr.* **1995**, *T57*, 117.

(53) Walters, J. K.; Rigden, J. S.; Newport, R. J. *Phys. Scr.* **1995**, *T57*, 137.

(54) Swenson, J.; Börjesson, L.; McGreevy, R. L.; Howells, W. S. *Physica B* **1997**, *234*, 386.

(55) Hansen, L. B.; Stoltze, P.; Nørskov, K.; Clausen, B. S.; Niemann, W. *Phys. Rev. Lett.* **1990**, *64*, 3155.